Nanoscale

Accepted Manuscript

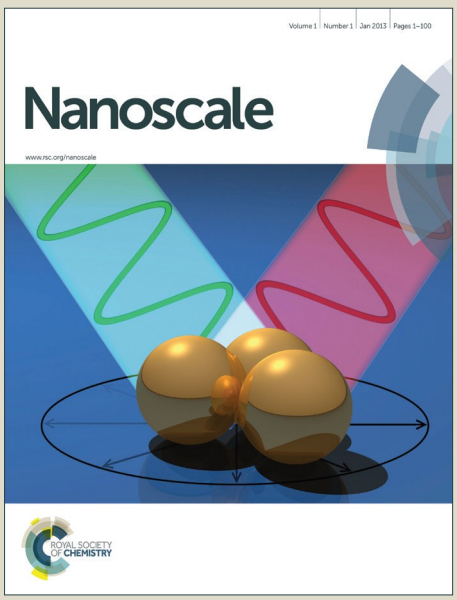

ROYAL SOCIETY OF CHEMISTRY

www.rsc.org/nanoscale

A Nanodrop on the Surface of a Lubricating Liquid Covering a Rough Solid Surface

Gersh O. Berim and Eli Ruckenstein*

Department of Chemical and Biological Engineering,

State University of New York at Buffalo,

Buffalo, New York 14260

August 19, 2015

*Author to whom correspondence should be addressed. Electronic mail: feaeliru@buffalo.edu; Phone number: (716)645-1210; Fax: (716)645-3822.

Abstract

A two-component fluid consisting of a lubricating fluid (LF) that covers a rough solid surface (surface decorated by periodic array of identical pillars) and a test fluid (TF) as a nanodrop over LF is considered. A horizontal external perturbative force is applied to TF and the density functional theory is used for the treatment of the system. The concepts of advancing and receding contact angles as well as of leading edges of the drop are revisited. Three different definitions of the contact angles are analyzed and the most plausible selected. The contact angles are calculated as functions of drop size and magnitude of the perturbative force. For small drops, both angles change nonmonotonously with increasing perturbative force. For larger drops, the advancing contact angle has the tendency to increase and the receding contact angle to decrease with increasing force. The sticking force which maintains the drop equilibrium in the presence of an external perturbative force is determined as function of the contact angles. It is shown that this dependence is similar to that for a drop on a rough solid surface in the absence of LF. A critical sticking force, defined as the largest value of the perturbative force for which the drop remains at equilibrium, is determined.

1 Introduction

In paper [1], a nanodrop located on the smooth surface of a solid possessing hidden roughness was considered on the basis of the density functional theory (DFT). One of its goals was to use a microscopic approach to describe (qualitatively) the experimental results

[2]-[9] regarding the slipping of a nanodrop on a SLIPS (slippery liquid-infused porous surface). The main feature of SLIPS, which is interesting for practical applications, is the extremely small inclination angle at which the drop starts to slip along the surface of the lubricating liquid. This angle remains small both for large ($\theta > 90^\circ$) and small ($\theta < 90^\circ$) contact angle θ of the drop. The lubricating fluid, that covers in those experiments the rough solid surface, was modeled in Ref. [1] by a nonuniform second solid material possessing a smooth surface which generated, together with the rough substrate, an interaction potential acting on the drop of the test fluid (TF). Even though this approximation changes considerably the original system, it led to reasonable values for the slipping angle (the inclination angle of the surface when slipping begins).

In the present paper, a more realistic model consisting of a lubricating fluid (LF) that covers the rough surface of a substrate and a nanodrop of TF located onto LF is examined using the two-component DFT. A perturbative external force $\mathbf{F}_\tau$ acting on the molecules of TF is added in the horizontal direction. This force is balanced by a sticking force $\mathbf{F_{st}}$ which maintains the drop equilibrium. Schematically, the considered case is sketched in Figure 1 where, for simplicity, the nonuniformities of TF and LF are not indicated.

Such a model which, to our best knowledge was never considered microscopically, has several new features compared with the traditional one-component liquid drop on a solid surface. First, the latter is surrounded by a vapor of the same fluid which has a much smaller density compared to that of the drop. For this reason, the vapor-liquid interaction plays a minor role in the formation of the drop. In the present model, the environment of the drop includes a low density mixture of TF and LF around the upper part of the drop

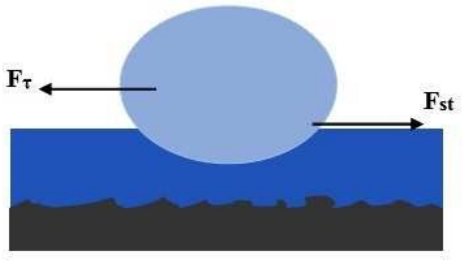

Figure 1: Schematic representation of a drop of the test fluid (light gray area), lubricating fluid (darker gray area), and rough substrate (black area). $\mathbf{F}_\tau$ is the horizontal perturbative force and $\mathbf{F}_{st}$ is sticking force which maintains the drop equilibrium.

(which has a negligible role in the formation of the drop) and a dense LF beneath the drop. The interaction between the latter part of LF and TF is responsible for the drop shape and location. In this case, the bottom part of the drop profile is not planar and this rises questions about the definition of the contact angle between the nanodrop and LF and the location of the leading edges of the nanodrop. (Note, that the drop has no direct contact with the solid and interacts with it indirectly via the LF). Another feature is that the contact between the nanodrop and LF occurs in the region of the LF-TF interface, i.e. in the region where the densities of LF and TF are nonuniform both in the vertical and horizontal directions with respect to the solid substrate. For this reason and because the thickness of LF-TF interface is comparable with the size of the drop, additional difficulties arise in the definition of the contact angle.

The goal of the present paper is to examine microscopically the new kind of systems using reasonable definitions of the quantities which characterize the drop of TF located

on LF. In Sec. 2, the system is defined in more details including the interaction potentials and the basic equations for the fluid density distributions. In Sec. 3, the drop profile is calculated, contact angles are defined and the results of the calculation of the contact angle and sticking force are provided along with their discussion.

2 The system and basic equations

2.1 The system

2.1.1 Geometry

The three components involved in our considerations are presented in Figure 2. The first component is the rough substrate of constant density ρ_s, its roughness being modeled by regular arrays of pillars of height h_p, width d_p and distance between pillars Δ_p. All distances between surfaces are measured between the centers of the molecules of their first layer. The pillars are infinite in the y-direction (normal to the plane of the figure). The second component, the lubricating fluid (LF), forms a nonuniform layer of liquid-like density on the surface of the substrate. Outside this layer, the LF is present in small amounts as a mixture with TF. The last component is the test fluid (TF) which forms a two-dimensional (cylindrical) drop extended in the y-direction. Outside the drop, TF is present in small concentrations as a mixture with LF. Evidently, a small amount of LF is also present in the drop, and a small amount of TF is present in the LF layer.

The upper boundary of the system is located at the distance h_u from the upper surface

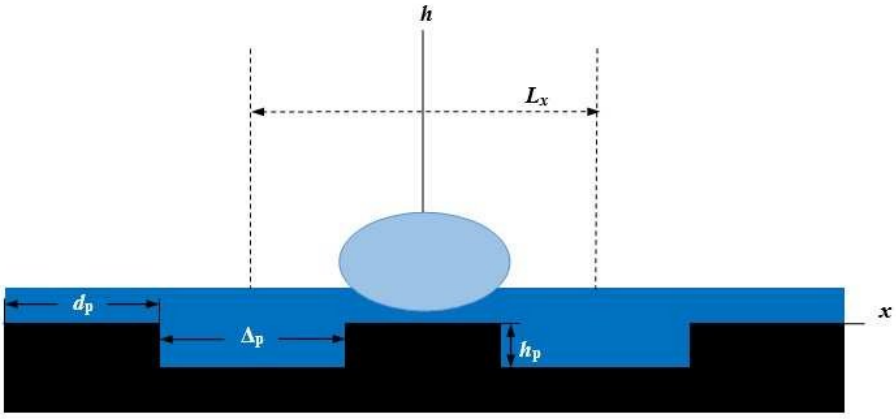

Figure 2: Schematic representation of the considered system which consists of a solid (substrate and pillars) of constant density (black area) covered by the lubricating fluid (lighter area), and the drop of the test fluid (light area). The lengths d_p, h_p, and Δ_p are the pillars width, height, and distance between pillars, respectively, $L_x = d_p + \Delta_p$ is the width of the unit cell used in the calculations. All distances between surfaces are measured between the centers of the molecules forming the first layers of the corresponding surfaces. The x-axis passes through the centers of the molecules of the lubricating fluid located next to the upper surface of pillars.

of the pillars and is treated as a hard wall (not shown in Figure 2). Because of the low densities of TF and LF close to the upper boundary, the influence of the latter on the state of the system is neglected. The system is periodic in the x-direction with period L_x, with the number of molecules of LF and TF per L_x constant (closed system).

It is supposed that there is no symmetry breaking in the y-direction and that the density distributions (FDDs) of LF ($\rho_1(\mathbf{r})$) and TF ($\rho_2(\mathbf{r})$) are uniform in this direction and non-uniform in the x- and h-directions, hence $\rho_i(\mathbf{r}) \equiv \rho_i(x,h)$ $(i = 1, 2)$.

2.1.2 Interaction potentials

It is supposed that the spherical molecules of LF and TF interact via a truncated Lennard-Jones potential

$$\phi_{ij}(r) = \begin{cases} \infty, & r \leq \sigma_{ij} \\ 4\epsilon_{ij}\left[\left(\frac{\sigma_{ij}}{r}\right)^{12} - \left(\frac{\sigma_{ij}}{r}\right)^{6}\right], & \sigma_{ij} < r \leq r_{ij,cut} \\ 0, & r > r_{ij,cut} \end{cases} \quad (1)$$

where i and j take the values 1 and 2 for LF and TF, respectively, r is the distance between the centers of a pair of interacting molecules, and $r_{ij,cut} = 3\sigma_{ij}$ is the cutoff distance. In eq 1, σ_{ij} and ϵ_{ij} are the hard core diameters and energy parameters, respectively. The molecules of TF and LF interact also with the rough solid (substrate plus pillars) of constant density which is considered as the source of an external potential which has the same form as eq 1 with no upper bound for the radius of the fluid-solid interactions. For these interactions, the hard core diameters σ_{ij} and interaction parameters ϵ_{ij} should be

replaced with σ_{is}, and ϵ_{is}, respectively, the subscript s indicating the solid.

It is also assumed also that each molecule of TF is exposed to a constant external perturbative force f_τ which acts in the negative direction of the x- axis.

As a result, the net external potential, $U_{net,ext}(x,h)$ has the form

$$U_{net,ext}(x,h) = U_{1s}(x,h) + U_{2s}(x,h) + U_e(x) \tag{2}$$

where $U_{is}(x,h)$ $(i=1,2)$ are potentials due to TF-solid and LF-solid interactions, respectively and $U_e(x) = f_\tau x$ is the potential due to the external perturbative force. For more details, one can see the Supplementary Material. Note that at equilibrium, the magnitude of the sticking force $F_{st} = f_\tau N_d$ where N_d is the number of molecule of TF in the drop. (Both F_{st} and N_d are calculated per unit length of the drop in y-direction.)

2.1.3 Selection of the parameters

Below, all lengths will be provided in units of TF-TF hard core diameter, $\sigma \equiv \sigma_{22}$. In this units, the geometrical characteristics of the system were selected as follows: $h_p = 3$, $d_p = 2$, $\Delta_p = 6$, $L_x = 24$, and $h_u = 16$.

The hard core diameters of all intermolecular interactions were considered equal ($\sigma_{11} = \sigma_{22} = \sigma_{12} = \sigma_{1s} = \sigma_{2s} \equiv \sigma = 3.405$Å).

The energy parameters of the potentials of the fluid-fluid interactions have the values $\epsilon_{11}/k_B = \epsilon_{22}/k_B \equiv \epsilon/k_B = 119.76$K, and $\epsilon_{12} = 0.5\epsilon$, where k_B is the Boltzmann constant. For the fluid-solid interactions the energy parameters were selected as $\epsilon_{1s} = 4\epsilon$ and $\epsilon_{2s} = 0$, respectively. The TF-solid interaction is neglected because of the large distance between

the drop and solid due to the presence of LF. The selected interaction parameters ϵ_{11}, ϵ_{22}, and ϵ_{12} provided the immiscibility of the two components, hence the existence of a drop of TF. In addition, the value employed for the energy parameter ϵ_{1s} allows the lubricating fluid to wet the solid completely forming a liquid layer that covers the pillars. The number density of the solid was taken $\rho_s = 1.92 \times 10^{28}\mathrm{m}^{-3}$ and the masses of the molecules of TF and LF were $m_1 = m_2 = 6.63 \times 10^{-26}\mathrm{kg}$. The temperature was selected $T = 87.3\mathrm{K}$.

2.2 The Euler-Lagrange equations for the fluid density distributions

The density distributions $\rho_i(\mathbf{r})$ $(i = 1, 2)$ are calculated using the density functional approach formulated by Rosenfeld [10]. As shown in Refs. [11]-[14] , the density functional theory, developed originally for open systems (grand canonical ensemble), can be also applied to closed systems (canonical ensemble). The only restriction, which is fulfilled by the present calculations, is the number of molecules to be sufficiently large. A detailed discussion regarding the applicability of the canonical ensemble DFT can be found in Ref. [15].

The total Helmholtz free energy $F_{tot}[\rho_1(\mathbf{r}), \rho_2(\mathbf{r})]$ can be expressed as the sum of an ideal gas free energy, $F_{id}[\rho_1(\mathbf{r}), \rho_2(\mathbf{r})]$, an excess free energy $F_{ex}[\rho_1(\mathbf{r}), \rho_2(\mathbf{r})]$, and a free energy $F_{1s}[\rho_1(\mathbf{r})] + F_{2s}[\rho_2(\mathbf{r})]$ due to the interactions between fluids and solid. Minimization of the $F_{tot}[\rho_1(\mathbf{r}), \rho_2(\mathbf{r})]$ leads to a system of two Euler-Lagrange equations for the FDDs $\rho_i(x, h)$ $(i = 1, 2)$

$$\log[\Lambda_i^3 \rho_i(\mathbf{r})] - Q_i(\mathbf{r}) = \lambda_i / k_B T, \quad (i = 1, 2) \tag{3}$$

where $\Lambda_i = h_P/(2\pi m_i k_B T)^{1/2}$ is the thermal de Broglie wavelength of the molecules of component i, h_P is the Planck constant, T is the absolute temperature, m_i is the molecular mass of component i, $Q_i(\mathbf{r})$ is a functional of the densities $\rho_i(\mathbf{r})$ and λ_i is a Lagrange multiplier arising because of the constraint of fixed average density of component i in the system

$$\rho_{i,av} = \frac{1}{V_i} \int_{V_i} d\mathbf{r} \rho_i(\mathbf{r}) \tag{4}$$

where V_i is the volume of the system accessible to component i.

Using eqs 3 and 4, the Lagrange multipliers can be rewritten in the form

$$\lambda_i = -k_B T \log \left[\frac{1}{\rho_{i,av} V_i \Lambda_i^3} \int_{V_i} d\mathbf{r} e^{Q_i(\mathbf{r})} \right] . \tag{5}$$

By eliminating λ_i between eqs 3 and 5, one obtains two integral equations for the FDDs $\rho_1(x, h)$ and $\rho_2(x, h)$ which can be solved by numerical iterations.

The details of the derivation of the Euler-Lagrange equation and of the numerical procedure used for their solutions are provided in the Supplementary Material.

3 Results and discussion

Below, five specific cases, C_m $(m = 1, ..., 5)$, are considered which differ from each other by the average number densities $\rho_{i,av}$ $(i = 1, 2)$ and, as a consequence, by the numbers

Table 1: Average number densities $\rho_{1,av}$ and $\rho_{2,av}$ of LF and TF, respectively for five considered cases

Case	C_1	C_2	C_3	C_4	C_5
$\rho_{1,av}\sigma^3$	0.175	0.211	0.211	0.211	0.250
$\rho_{2,av}\sigma^3$	0.075	0.075	0.105	0.120	0.075

of molecules of TF and LF in the system. In Table 1, the dimensionless values, $\rho_{i,av}\sigma^3$ $(i = 1, 2)$, are listed for all five cases. The results obtained for each of these cases will be used below to analyze the characteristics of the drop for various thicknesses of LF and various sizes of the drop.

3.1 Density distributions of the test and lubricating fluids and the drop profile

In Figure 3, various FDDs of TF and LF are presented for the case C_3 and for $f_\tau = 1.36 \times 10^{-15}$N. Because of the nonzero horizontal perturbative force, the drop location is displaced to the left of the middle of the pillar. For this reason, LF and TF densities at the left hand side of the drop is slightly (not detectable by eye) different from those on the right hand side, so the drop is slightly asymmetric. Figure 3a, presents the two-dimensional FDD of TF calculated using eq 3. The white dashed solid line in this figure represents the profile of a drop which was obtained using a procedure similar to that for a drop on a solid surface (see e.g. Ref. [1]). According to that procedure, the drop profile is defined as a line along which the local density of TF $\rho_2(x, h)$ is constant and equal to the

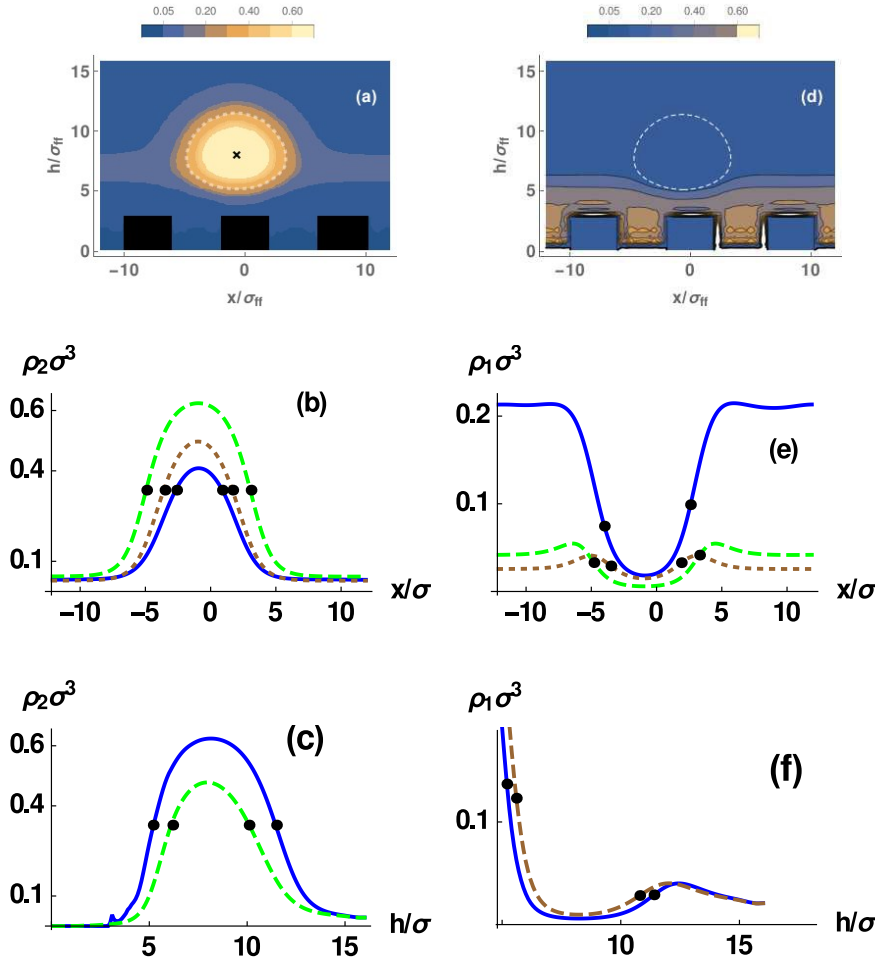

Figure 3: Various FDDs of TF and LF for the case C_3 and $f_\tau = 1.36 \times 10^{-15}$N. (a) and (d) Two-dimensional density distributions of TF and LF, respectively. The cross in panel (a) indicates the location of the maximum density of TF inside the drop. The white lines indicate the drop profile; (b) TF density distributions along the horizontal lines at the distances 2.5 (solid line), 5.0 (dashed), and 8.0 (dotted) from the upper surface of the pillars. (c) TF density distributions along the vertical lines passing through the point of maximum density of TF (solid line) and midway between pillars (dashed line). Curves in panels (e) and (f) represent similar FDDs as in (b) and (c) for LF.

TF density at the location of the equimolar dividing surface of a horizontal FDD $\rho_2(x, h_0)$ at some distance h_0 from the upper surface of the pillars, by considering this FDD as that of a planar vapor-liquid interface. In the present paper, the horizontal FDD was taken along the line passing through the location of the maximum TF density (cross in Figure 3a). In this case, the density $\rho_{2,div}$ of TF on the dividing surface is $\rho_{2,div}\sigma^3 = 0.336$. After the profile is determined, other characteristics of the drop, such as, for example, the number of molecules in the drop (drop size) can be calculated [16].

Several examples of one-dimensional density distributions of TF along the horizontal and vertical lines are presented in Figures 3b and c, respectively, in the region of the drop location. The points on each curve represent the locations of the drop profile for the corresponding one-dimensional FDD. All presented FDDs are slightly asymmetrical with respect to the vertical line passing through their maximum. For the horizontal FDDs, this asymmetry is due to the presence of pillars and external force f_τ , and for vertical FDDs to the increasing distance from the solid.

Similar density distributions for LF are displayed in Figures 3d,e,f. One can see that LF penetrates into the drop, its density decreasing with increasing distance from the drop surface. However, the fraction of LF molecules inside the drop is about 4.7% of the total number of molecules in the drop. This fact justifies the neglect of the action of the external perturbative force on the molecules of the lubricating fluid.

Let us note that in all considered cases only the stable nanodrops were analyzed. In the absence of an external force, those drops are centered on the pillars. The drops which are centered between neighboring pillars were metastable (had greater free energy than

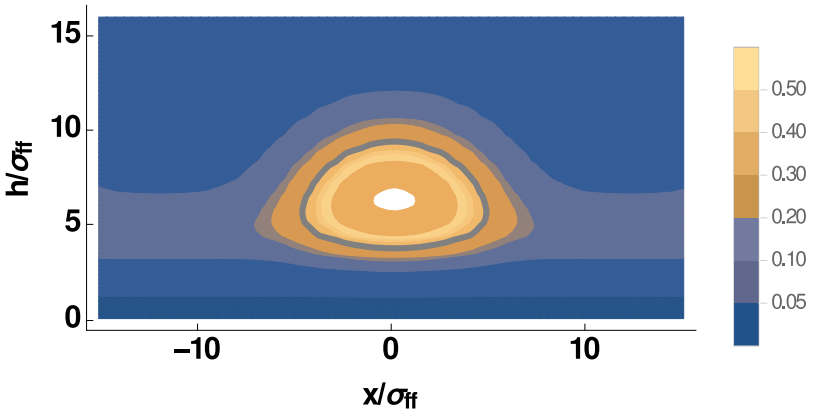

Figure 4: Dimensionless density distribution ($\rho(x,h)\sigma^3$) of the test fluid for a smooth solid surface at $\rho_{1,av}\sigma^3 = 0.211$, $\rho_{2,av}\sigma^3 = 0.120$, and $\epsilon_{12}/\epsilon_{22} = 0.6$. The black line in this figure represents the drop profile obtained by the procedure described in Sec. 3.1.

the stable ones) at $f_\tau = 0$ and unstable at $f_\tau \neq 0$. Other solutions of Euler-Lagrange equations were not found.

3.2 Contact angle

Due to the nonplanar shape of the bottom part of the drop and, as a result, the absence of a fixed reference surface (such as, e.g., the surface of the solid), the definition of leading edges of the drop and the contact angle which the drop makes with the reference surface is not straightforward and unique. To make a reasonable choice, let us consider for simplicity the specific case of a nanodrop on the surface of a lubricating fluid that covers a smooth solid surface. The density distribution of the test fluid in such a system is presented in Figure 4. Below, several possibilities are examined regarding the reference line with which the profile (or its extension) intersects to form an angle which can be considered as the contact one.

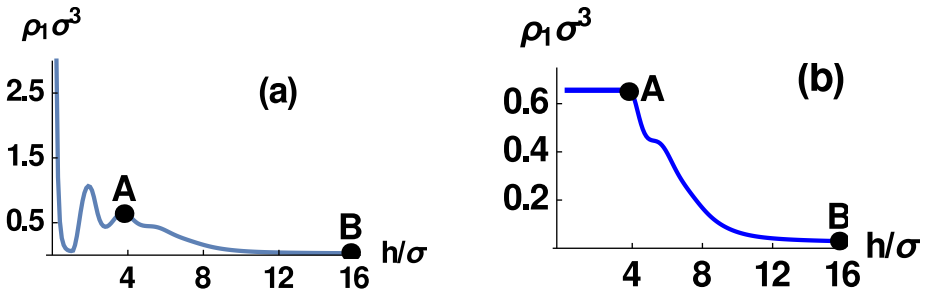

Figure 5: (a) Density distribution of the lubricating fluid along the vertical line passing through the point of maximum density of the test fluid in the drop. At points A and B, the density of LF has liquid-like and vapor-like values, respectively. (b) Fictitious density distribution of the lubricating fluid which was used to find the equimolar dividing surface.

Definition 1: Similar to the drop profile, the surface of the lubricating fluid can be considered as the line along which the density of LF is a constant equal to the density of LF on the dividing surface of a particular one-dimensional density distribution of LF. The latter distribution is considered to be along the vertical line passing through a point inside the drop where the density of the test fluid has a maximum. Because of the oscillating behavior of the LF density close to the wall (see Figure 5a), a special procedure to find the dividing surface which separates the vapor and liquid phases, should be developed. In the present case, we select the part of the FDD between points A and B (see Figure 5a) and replace the actual FDD with one presented in Figure 5b. (At points A and B, the density of LF has liquid-like and vapor-like values, respectively.) This FDD is used to find the location of the equimolar dividing surface and the density of LF at that location.

In Figure 6, the drop profile and the defined surface of LF (solid curve beneath the drop) are presented. One can see that the drop profile and the surface of LF do not

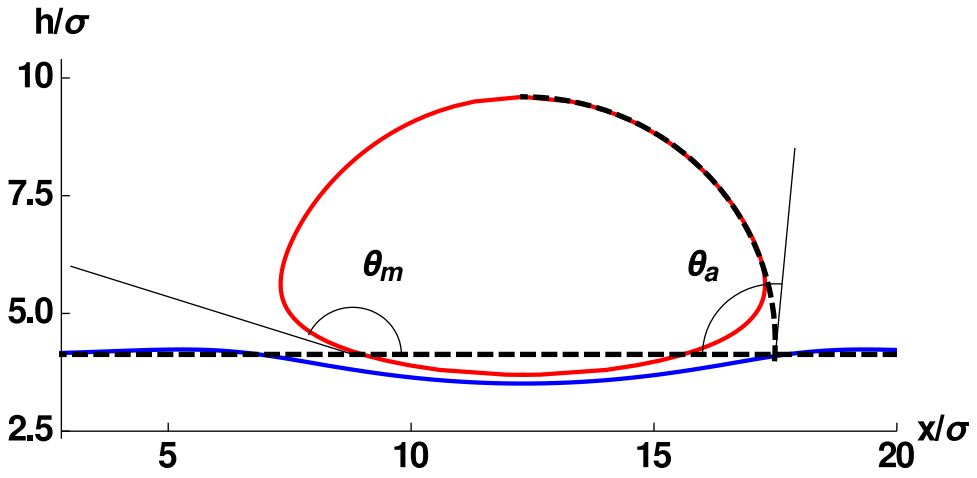

Figure 6: Microscopic (θ_m) and apparent (θ_a) contact angles according to Definition 1. The surface of the lubricating fluid (LF) (the solid curve beneath the drop) is obtained using the LF density on the dividing surface for one-dimensional density distribution of LF along the vertical line passing through the center of the drop (point of maximum density of the test fluid).

intersect and this can be interpreted that between the drop and the surface of LF there is a thin layer of a low density mixture of TF and LF. The reference line was selected as the horizontal line which far from the drop coincides with the surface of the lubricating fluid. This line is presented as the dashed one in Figure 6. After the reference line is introduced, one can define two types of contact angles which characterize the nanodrop. The first, θ_m, which can be called microcontact angle [17], is defined using the part of the drop profile in Figure 6 in the vicinity of the reference line (see the left hand side of Figure 6). The second, the apparent contact angle θ_a, is defined using a circular extension of the upper part of the drop profile (see right hand side of Figure 6).

Definition 2: Similar to Definition 1, the surface of the lubricating fluid can be considered as a line of constant density. However, this density is selected as the density of LF

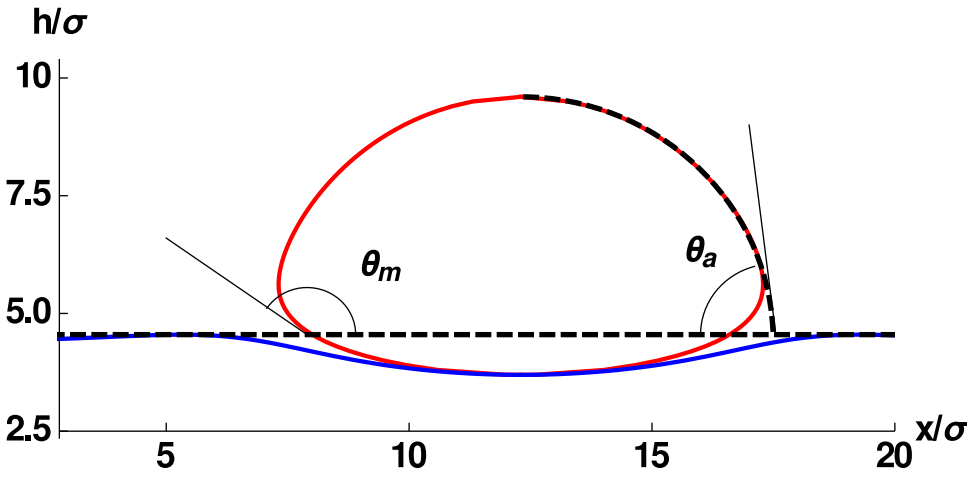

Figure 7: Microscopic (θ_m) and apparent (θ_a) contact angles according to Definition 2. The surface of the lubricating fluid (LF) (the solid curve beneath the drop) is obtained using the LF density at the lowest point of the drop profile.

at the location of the lowest point of the profile. The micro- and apparent contact angles obtained according to this definition are presented in Figure 7.

Definition 3: Another possible definition of the contact angles is to consider that the reference line passes through a characteristic point of the drop. As such a point, one can select, for example, the point inside the drop where the density of TF has a maximum (see Figure 8). In this case, the microscopic and apparent contact angles practically coincide ($\theta_m = \theta_a = \theta$).

For a smooth solid surface, the contact angles obtained for a nanodrop in the system with $\rho_{1,av}\sigma^3 = 0.211$, $\rho_{2,av}\sigma^3 = 0.120$ and various values of ϵ_{12} are provided in Table 2. One can see that different definitions provide very different values of the contact angles.

Even though the first definition appears to be the most natural one, we will select below Definition 2. The reason is that the practical realization of Definition 1 is not

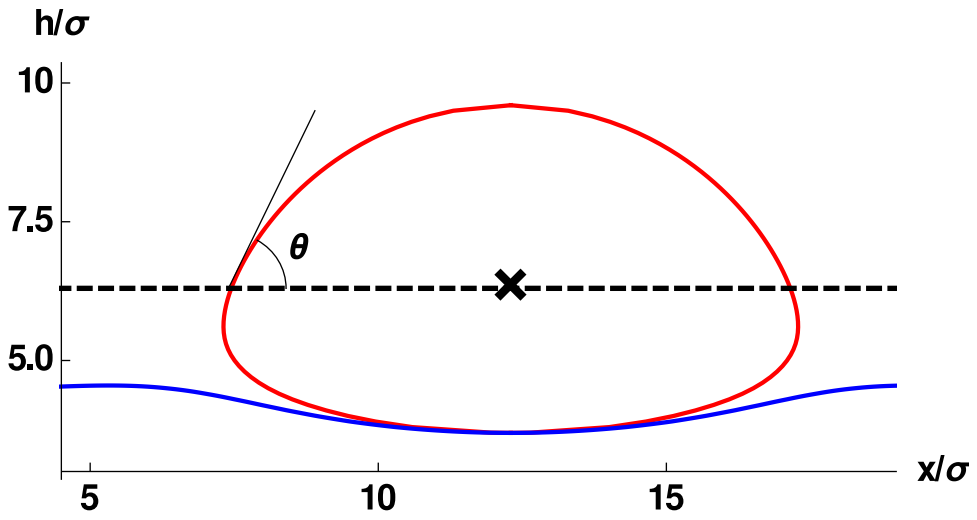

Figure 8: Contact angle θ according to Definition 3. The cross indicates the point where the density of TF has a maximum. The surface of the lubricating fluid (LF) (the solid curve beneath the drop) does not participate in forming θ.

Table 2: Microscopic (Θ_m) and apparent (Θ_a) contact angles calculating according to various definitions for smooth solid surface and $\rho_{1,av}$ =0.211, $\rho_{2,av}$ =0.120, and various values of ε_{12}. (The latter parameter is provided in units of ε_{22}.)

	Definition 1		Definition 2		Definition 3
$\varepsilon_{12}/\ \varepsilon_{22}$	Θ_a	Θ_m	Θ_a	Θ_m	Θ
0.5	120.1	169.6	110.3	142.5	79.9
0.55	106.9	163.3	100.9	144.2	75.6
0.6	93.3	160.1	90.0	148.2	70.3
0.65	82.6	176.0	75.6	156.1	60.1

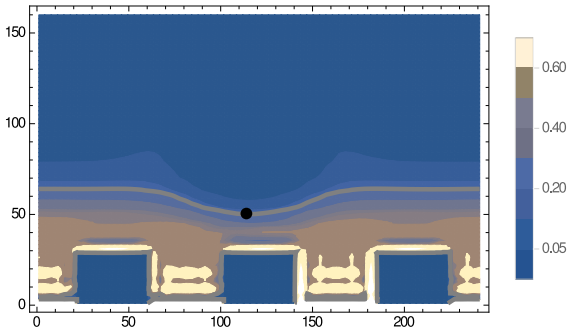

Figure 9: FDD of LF for the case C_3 and $f_\tau = 1.36 \times 10^{-15}$N. The dot indicates location of the lowest point of the drop profile and the thick line represent the line of constant density of LF passing through this point. The magnitude of the fluid density is provided in dimensionless form as $\rho_2(x,h)\sigma^3$.

straightforward because of the uncertainty in the selection of point A on the actual density profile (see Figure 5 that leads to uncertainty in determining the location of the equimolar dividing surface. Definition 3 does not take explicitly into account the presence of LF and for this reason seems to be inappropriate.

It is obvious that the microcontact angle depends stronger on the TF-LF interactions than the apparent one. For this reason, below only the microcontact angle will be used.

Let us consider the application of Definition 2 to a rough surface using as an example case C_3. For this case, FDD of LF is presented in Figure 9. The dot in this figure provides the location of the lowest point of the drop profile and the thick line represents the line of constant density of LF passing through this point. The part of this line far from the drop is almost straight and its extension will be used as the reference line for the definition of the leading edges and advancing (θ_1) and receding (θ_2) contact angles in the way illustrated in Figure 10. In the latter figure, the reference line is represented by the dashed line and points A and R indicate the locations of the advancing and receding

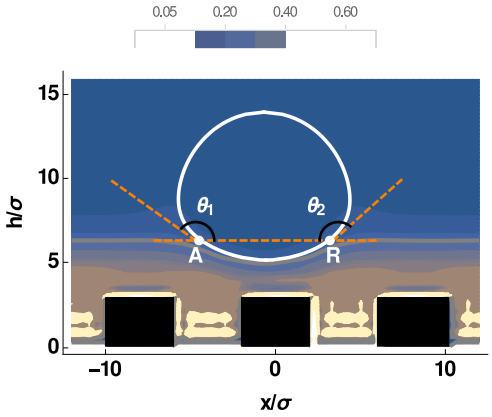

Figure 10: FDD of LF for the case C_3 and $f_\tau = 1.36\times10^{-15}$N and profile of the drop of TF (closed white line) along with the reference line (dashed line) defined as noted in the text. θ_1 and θ_2 are considered as advancing and receding contact angles and points A and R as locations of the leading edges of the drop.

leading edges of the drop.

Following the definition of contact angle, the dependence of θ_1 and θ_2 on the size of the drop and on the magnitude of the perturbative force were calculated.

In Table 3, the contact angles and sizes of the drop are presented for cases $f_\tau = 0$, $f_\tau = 1.36\times10^{-15}$N and $\rho_{1,av}\sigma^3 = 0.211$. In all cases, the magnitudes of the contact angles

Table 3: The values of the contact angles for different drop sizes at $f_\tau = 0$ and $f_\tau = 1.36\times10^{-15}$N. ($\rho_{1,av}\sigma^3 = 0.211$)

$N_d\sigma$	$f_\tau = 0$		$f_\tau = 1.36\times10^{-15}$N	
	$\theta_A(deg)$	$\theta_R(deg)$	$\theta_A(deg)$	$\theta_R(deg)$
8.8	127.1		133.5	131.9
19.8	122.5		123.5	121.8
24.9	121.8		122.1	120.0

decrease with increasing drop size. In previous papers [1, 18] in which a drop in contact with a rough surface was considered, such a dependence of the contact angle was explained by the change of the location of the leading edges of the drop with respect to the potential

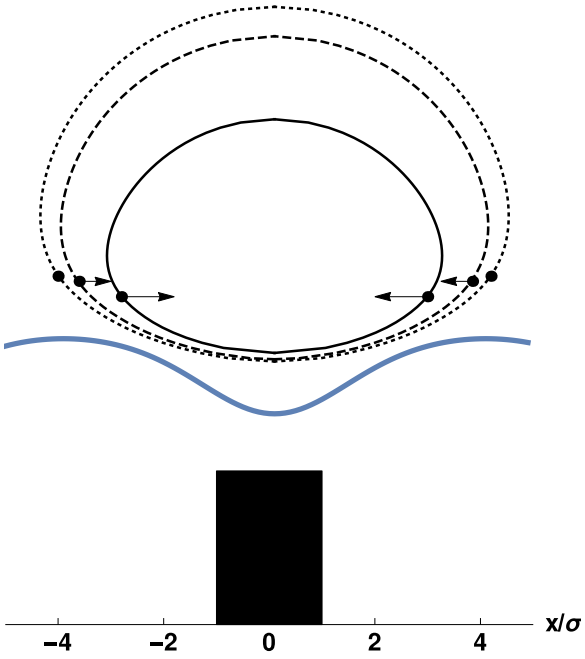

Figure 11: Drop profiles (closed lines) and profile of the potential (in arbitrary units) generated by a rough solid (thick line). The solid, dashed, and dotted profiles correspond to drops with $N_d = 8.8$, 19.8, and 24.9, respectively. The dots and arrows indicate the locations of the leading edges of the drop and the forces on them due to the interaction with the solid, respectively.

of the liquid-solid interactions. In the system considered in the present paper, the drop has no direct contact with the solid and the molecules of TF do not interact with the solid ($\epsilon_{2,s} = 0$). The solid affects the drop indirectly through its interaction with LF, the latter interacting with the molecules of TF. The largest contribution to this interaction comes from the molecules of LF closest to the drop. The larger the density of those molecules, the greater is the net TF-LF interaction.

In Figure 11, three drop profiles corresponding to drops of different sizes at $f_\tau = 0$ are presented along with the locations of the leading edges of the drop defined as described above. The thick line represents the behavior of the potential (given in arbitrary units)

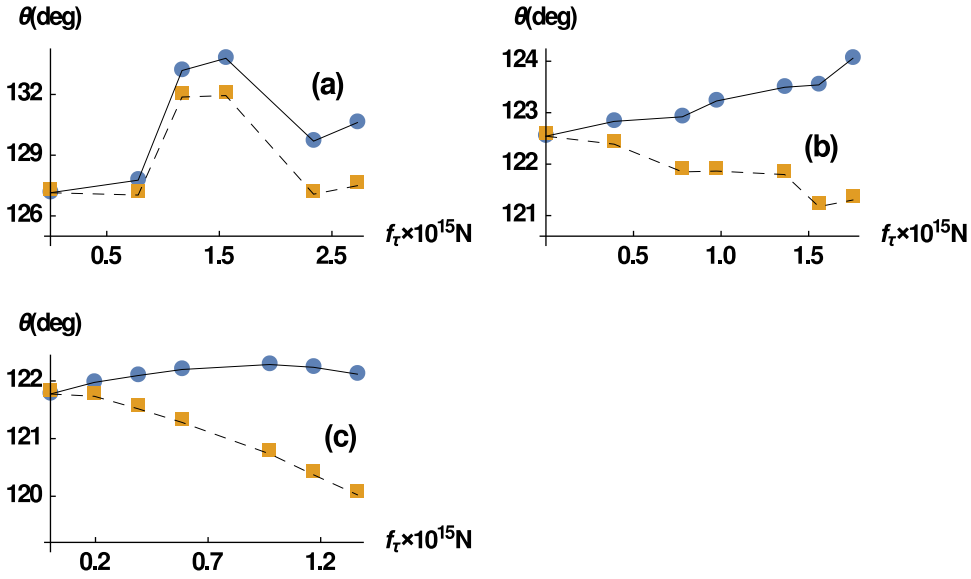

Figure 12: Calculated advancing (points) and receding (squares) contact angles as functions of external perturbative force for cases C_2 (a), C_3 (b), and C_4 (c). The lines are guides for eye.

generated by the rough solid in the vicinity of the drop. The magnitude of the potential has its largest value located above the middle of the pillar (note that the potential is negative). The calculations show that the LF density behaves similar to the potential and, hence, the behavior of LF - drop interaction is also similar to that of the potential. With increasing size of the drop, the leading edges are displaced to the region of weaker horizontal interaction forces (which are defined by the horizontal component of the gradient of the interaction potential and are represented by the arrows in the figure) between TF and LF. The decrease of those forces favors the increase of the bottom area of the drop and the decrease of the contact angle.

In Figure 12, the dependencies of the advancing and receding contact angles on the magnitude of the perturbative force f_τ is presented for cases C_2, C_3 and C_4. As

expected, in all cases, the difference between θ_1 and θ_2 increases with increasing f_τ. For larger drops (cases C_3 and C_4), the receding angle θ_2 has the tendency to decrease with increasing f_τ while the advancing angle θ_1 has the tendency to increase. For smaller drops, the dependence of the contact angles on f_τ is not monotonous.

3.3 Sticking force

As discussed in Ref. [1], where a drop on the smooth surface of a second solid material (SSM) covering a rough solid was examined, the microscopic origin of the sticking force acting on the drop of TF is the external potential generated by the rough solid, which is nonuniform both in the horizontal and vertical directions. In the case considered in the present paper, the role of SSM is played by a lubricating fluid which interacts with the rough solid and with TF. The former interaction is responsible for the nonuniformity of LF which, in turn, generates a nonuniform potential acting on the drop. (One should note, that the interaction of TF with the solid in not taken into account in the present paper because it is negligible compared to that between LF and TF).

If, in the presence of an external perturbative force f_τ, the drop remains in mechanical equilibrium, the sticking force per molecule, $f_{st} \equiv F_{st}/N_d$, is equal to f_τ ($f_{st} = f_\tau$). The largest value of f_τ at which the drop remains in equilibrium (the solution of the Euler-Lagrange equations eq 3 does exist) is equal to the so called critical sticking force $f_{st,c}$ per molecule of the drop. Several values of the force $f_{st,c}$ along with the net critical sticking force per unit length in the y-direction $F_{st,c}$ are provided in Table 4.

Figure 13 represents the calculated sticking force as function of $\delta \equiv \cos\theta_2 - \cos\theta_1$ for

Table 4. Critical net sticking force, $F_{st,c}$, per unit length in y- direction and critical sticking force per molecule, $f_{st,c}$, for considered cases.

Case	$N_d\sigma$	$F_{st,c} \times 10^5$N/m	$f_{st,c} \times 10^{15}$N
C_1	8.04	9.66	4.09
C_2	8.94	7.17	2.72
C_3	19.89	10.22	1.75
C_4	24.85	9.93	1.36
C_5	9.88	3.94	1.36

different sizes of the drop and the same thickness of LF (cases C_2 (points), C_3 (squares), and C_4 (diamonds)). The lines are the best linear fits passing through the origin. The results are in agreement with the expression for a drop on a planar solid surface based on classical thermodynamics

$$F_{st} = C\gamma_{lv}(\cos\theta_2 - \cos\theta_1) \tag{6}$$

where C is a constant dependent on the drop shape, and γ_{lv} is the liquid-vapor surface tension [19, 20] which predicts a linear dependence of the sticking force on δ. (Note, that our previous study of a nanodrop on a rough surface in the absence of a lubricating fluid [1, 21] also provided a linear dependence between those two quantities.) Because for a macroscopic drop γ_{lv} as well as C (for a cylindrical drop) are constant the slope of the line does not depend on the size of the drop, and the sticking force is independent of the drop size. However for a nanodrop, one can see from Figure 13, that the slope of the dependence of F_{st} on δ decreases with increasing drop size (see Table 4 for drop sizes). In terms of macroscopic thermodynamics, such a behavior may be caused by the dependence

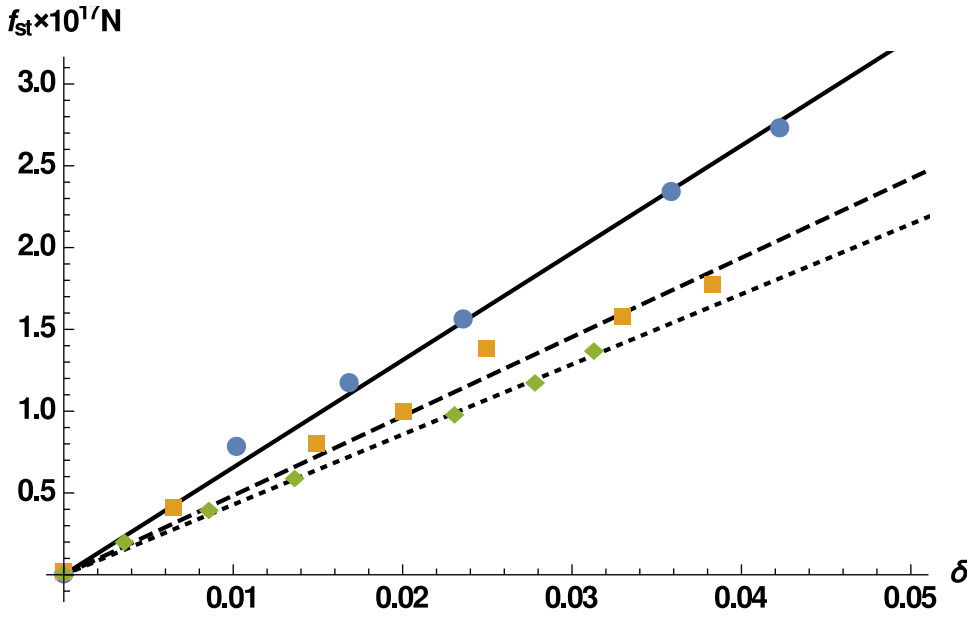

Figure 13: Dependence of the sticking force on $\delta = \cos\theta_2 - \cos\theta_1$ for the cases C_2 (solid line), C_3 (dashed), C_4 (dotted). The points, squares, and diamonds present results of calculations. The lines are the best linear fits passing through the origin.

of γ_{lv} on the distance from the upper surface of the pillars because of the dependence of the density of LF vapor on this distance.

In Figure 14 the best linear fits for the sticking force as function of δ are presented for different thicknesses of LF, which correlate with $\rho_{1,av}\sigma^3$ and for the same drop size ($N_d\sigma = 8.8$) (Cases C_1, C_3 and C_5). In this case, the increase of the thickness of the LF layer results first in a decrease of the slope of F_{st} vs δ dependence (transition from case C_1 (solid line) to case C_3 (dashed line) which is followed by the increase of this slope (transition from case C_3 to case C_5 (dotted line).

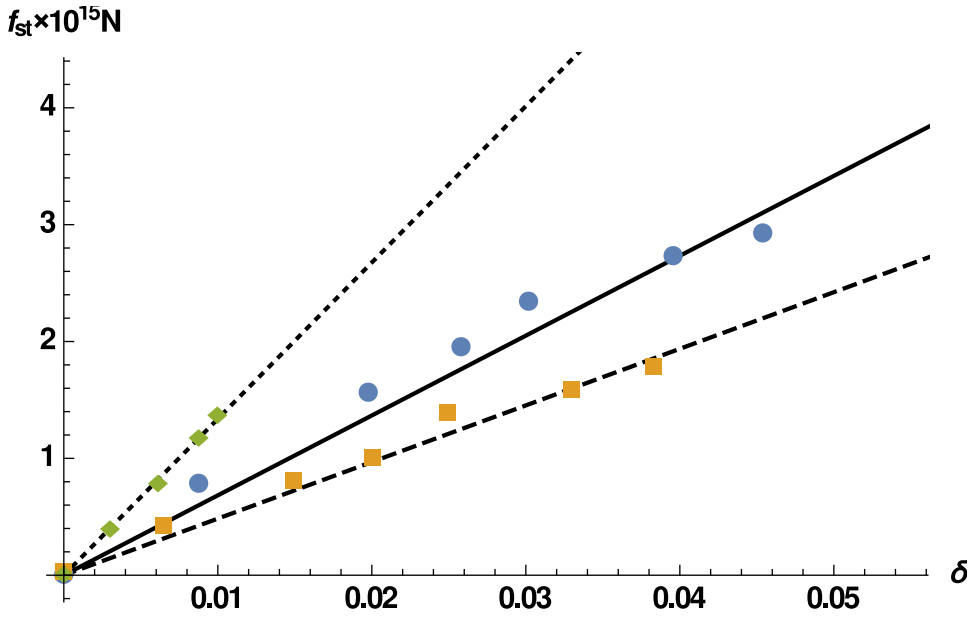

Figure 14: Dependence of the sticking force on $\delta = \cos\theta_2 - \cos\theta_1$ for the cases C_1 (solid line), C_3 (dashed), C_5 (dotted). The points, squares, and diamonds present results of calculations. The lines are the best linear fits passing through the origin. The thickness of the lubricating fluid is the smallest for case C_1 and largest for C_5.

4 Conclusion

In the present paper, a nanodrop on the surface of a lubricating fluid covering a rough solid surface is considered from a microscopic point of view on the basis of the two-component density functional theory in the presence of an external horizontal perturbative force. For such a system, the comparable values of the thickness of TF-LF interface and of the size of a nanodrop of TF on the surface of LF leads to uncertainty in the definition of the contact angles (advancing and receding) characterizing the nanodrop. Analyzing several possible definitions of the drop profile and of the surface of the lubricating fluid, the most plausible one was selected and the contact angles (advancing and receding) were calculated for various sizes of the drop as functions of the perturbative force. For smaller sizes, this dependence has a maximum, while for larger sizes of the nanodrop it is monotonous. This suggests, that there is a critical size of the drop at which the dependence of contact angles on the external force transforms from nonmonotonous to monotonous.

The sticking force which maintains the drop equilibrium is equal in magnitude and opposite in direction to the horizontal external force acting on the drop. It has a linear dependence on $\cos\theta_2 - \cos\theta_1$ which is similar to that for a macrodrop. The maximum possible sticking force (critical sticking force) was calculated as the largest external force at which the Euler-Lagrange equation has a solution.

It is natural to compare the obtained results with those obtained in Ref. [1] for a drop on a smooth surface of a solid material covering a rough surface. However because of the substantial difference of the considered systems and interaction parameters, a quantitative

comparison is impossible. For this reason, we restrict to a qualitative comparison of the results obtained in Ref. [1] and in the present paper.

Two main differences between the drop shapes and composition can be mentioned. A drop of a one-component fluid on the surface of a solid has a flat contact area with the solid and the fluid density distribution in the vertical direction is oscillatory close to the surface of the solid (see, for example, Fig. 6 in Ref. [1] and Fig. 5 in Ref. [16]). In contrast, a drop of a test fluid on the surface of a lubricating fluid has a nonplanar contact area and a nonoscillating behavior of the TF density distribution in the vertical direction (see Figures 3c,d and 4 of the present paper). Both differences occur because of a layering effect which plays a major role in the region of fluid-solid contact and is weak at a fluid-fluid interface.

References

[1] G.O.Berim and E.Ruckenstein, *Nanoscale*, 2015, **7**, 7873-7884.

[2] T.S.Wong, S.H.Kang, S.K.Y.Tang, E.J.Smythe, B.D.Hatton, A.Grinthal and J.Aizenberg, *Nature*, 2011, **477**, 443-447.

[3] W.Ma, Y.Higaki, H.Otsuka and A.Takahara, *Chemical Communications.*, 2013, **49**, 597-599.

[4] A.K.Epstein, T.S.Wong, R.A.Belisle, E.M.Boggs and J.Aizenberg, *Proceedings of the National Academy of Sciences of the United States of America.*, 2012, **109**, 13182-13187.

[5] P.W.Wilson, W.Z.Lu, H.J.Xu, P.Kim, M.J.Kreder, J.Alvarenga and J.Aizenberg, *Physical Chemistry Chemical Physics*, 2013, **15**, 581-585.

[6] J.D.Smith, R.Dhiman, S.Anand, E.Reza-Garduno, R.E.Cohen, G.H.McKinley and K.K.Varanasi, *Soft Matter.*, 2013, **9**, 1772-1780.

[7] R.Qiu, Q.Zhang, P.Wang, L.Jiang, J.Hou, W.Guo and H.Zhang, *Coll. Surf. A*, 2014, **453**, 132-141.

[8] L.Xiao, J.Li, S.Mieszkin, A.Di Fino, A.S.Clare, M.E.Callow, J.A.Callow, M.Grunze, A.Rosenhahn and P.A.Levkin, *ACS Applied Materials & Interfaces*, 2013, **5**, 10074-80.

[9] J.Li, T.Kleintschek, A.Rieder, Y.Cheng, T.Baumbach, U.Obst, T.Schwartz and P.A.Levki. *ACS Applied Materials & Interfaces*, 2013, **5**, 6704-6711.

[10] Y.Rosenfeld, *Phys. Rev. Lett.*, 1989, **63**, 980-983.

[11] A.González, J.A.White, F.L.Román and S.Velasco, *Phys. Rev. Lett.*, 1997, **79**, 2466-2469.

[12] A.González, J.A.White, F.L.Román and R.Evans, *J. Chem. Phys.*, 1998, **109**, 3637-3650.

[13] J.A.White and S.Velasco *Phys. Rev. E*, 2000, **62**, 4427-4430.

[14] J.A.White, A.González,F.L.Román and S.Velasco, *Phys. Rev. Lett.*, 2000, **84**, 1220-1223.

[15] A.V.Neimark, P.I.Ravikovitch, and A.Vishnyakov, J.Phys. Condens. Matter. **15**, 347 (2003).

[16] G.O.Berim and E.Ruckenstein, *J.Chem. Phys.*, 2008, **129**, 014708.

[17] C.A.Miller and E.Ruckenstein, *J.Colloid Interface Sci.*, 1974, **48**, 368; E.Ruckenstein and P.S.Lee, *Surf. Sci.*, 1975, **52**, 298.

[18] G.O.Berim and E.Ruckenstein, *Nanoscale*, 2015, **7**, 3088-3099..

[19] C.G.L.Furmige, J.Colloid.Sci., 1962, **17**, 309.

[20] M.Callies and D.Quéré, *Soft Matter*, 2005, **1**, 55.

[21] G.O.Berim and E.Ruckenstein, *J.Chem. Phys.*, 2008, **129**, 014709.